Phobos topography studying with tether system in elliptic restricted three-body problem

Vladimir S. Aslanov* and Anastasia V. Romanenko†
Samara National Research University, Samara 443086, Russia

The paper discusses the possibility of realizing a spacecraft-tether mission to study the surface of Phobos within the framework of the planar elliptic restricted three-body problem taking into account the topography of Phobos. The tether system is a weightless and inextensible tether with an instrument unit attached to it to study the surface of Phobos. Control laws of the tether length during deployment, the envelopment of the lunar surface by the instrument unit and the retraction of the tether system into the spacecraft are considered. The spacecraft is located in a low quasi-satellite orbit of Phobos. Four different altitude quasi-satellite orbits are analyzed with respect to the possibility to study the Phobos topography by means of the tether system. Numerical modelling confirms the effectiveness of the chosen nonlinear control laws of the tether system at all stages of motion.

Nomenclature

c = conservation of the angular momentum, $\mathrm{kg} \cdot \mathrm{m}^2 \cdot \mathrm{s}^{-1}$

d = distance between Mars and Phobos, m

f = true anomaly of the orbit of Phobos, rad

G = Newtonian gravitational constant, $6.67428 \cdot 10^{-11}$, $\mathrm{m}^3 \cdot \mathrm{s}^{-2} \cdot \mathrm{kg}^{-1}$

m_1 = mass of Mars, kg

m_2 = mass of Phobos, kg

m_3 = mass of the main spacecraft, kg

m_4 = mass of the instrument unit, kg

* Professor, Theoretical Mechanics Department, 34, Moscovskoe Shosse, aslanov.vladimir@gmail.com
† Undergraduate student, Theoretical Mechanics Department, 34, Moscovskoe Shosse, a-v-romanenko28@yandex.ru.

R = distance between the center of Phobos and the observation point on its surface, m

r = distance between Mars and Phobos, m

T = tension force, N

μ = $m_2 / (m_1 + m_2)$

Subscripts

1 = Mars

2 = Phobos

3 = spacecraft

4 = instrument unit

I. Introduction

For several decades Mars and its moons – Phobos and Deimos – have been of great scientific interest. Several missions to Mars and Phobos were designed since the eighties of the XX century [1-3]. Some launches were not that successful and the missions' development is continuing now. The beginning of one of such missions is assigned for 2026. Phobos is difficult to study because, due to its low density, Hill's spheres are partially inside its surface, so Keplerian orbits cannot be used [4]. In this case, a number of researchers are proposing the use of quasi-satellite orbits (QSOs). [5-11]. For instance, during the Martian Moons eXploration (MMX) mission developed by the Japan Aerospace Exploration Agency (JAXA) it is intended to use QSOs [8,12].

Tether systems are a prospective technology that can be generally applicable in interplanetary missions in the future. There are several books [13-15] and hundreds of articles [16-26] dedicated to tether systems and their implementation in space engineering. The characteristics of tethered systems, including their variable configuration, offer a wide range of applications in space technologies. The possibility of using a tether system to observe the surface or to deliver a rover on Phobos in MMX-type missions was explained in a paper by Aslanov [27]. The idea to which the paper [27] is dedicated consists of the following. A tether with an instrument unit attached to it is to be deployed to the Phobos surface from the spacecraft located on the QSO. The unit needs to reach the stated altitude of several dozen meters above the Phobos surface and make a complete revolution around it. After that the unit should be returned back on the spacecraft. Such an idea can become an addition to missions aimed at Martian moons investigation due to the fact that it does not require high additional costs. All in all, tether systems can be used in MMX-like missions for surface observation or rover delivery to Phobos.

However, in the paper [27], a number of questions remained unresolved. The motion of the spacecraft and the instrument unit was considered in terms of the circular restricted three-body problem (CR3BP). So, the influence of the eccentricity of the Mars-Phobos system on the motion of the spacecraft and the instrument unit was not taken into consideration. Also, the Phobos surface was approximated by an ellipse, and thereby the Phobos terrain was out of the examination. In addition, the motion of the spacecraft-tether system was only studied for a single orbit.

The present paper is a development of the research [27]; it focuses on the problem from the perspective of the elliptic restricted three-body problem (ER3BP), taking into account the topography of Phobos and considering several QSOs of various altitudes.

The implementation of the purpose is carried out in this paper in four stages:

1) The first stage is focused on the formulation of the basic assumptions and differential equations of motion in the framework of the elliptic restricted three-body problem. The construction of the curve to approximate the Phobos surface is under consideration.

2) In the second stage the numerical simulation of the tether deployment under the action of the linear control law is presented. It is shown that the linear control law is not effective for a new problem formulation.

3) The third stage is dedicated to the development of the nonlinear control law, which is effective for obtaining the desired instrument unit trajectories and conducting a designated study of the surface of Phobos.

4) In the fourth stage the numerical simulation of the tether retraction under the control law stabilizing the tether system is analyzed.

The scientific novelty of the work lies in the problem statement and the discussion of how the eccentricity of the Mars-Phobos system and the terrain of Phobos influence the motion of the spacecraft and the instrument unit. The construction of a nonlinear feedback control law for the deployment of a tether makes it possible to compensate for the influence of the eccentricity of the Phobos orbit and its terrain on the motion of the instrument unit attached to the tether when the control law is applied to the retraction of the tether within the framework of the introduced assumptions.

II. Key Assumptions and Equations of Motion

This section is dedicated to the derivation of the equations of motion of the spacecraft and the instrument unit in terms of ER3BP. In Fig. 1 the system consisted of the main spacecraft, the instrument unit and the tether is presented. The in-plane motion of the bodies is considered.

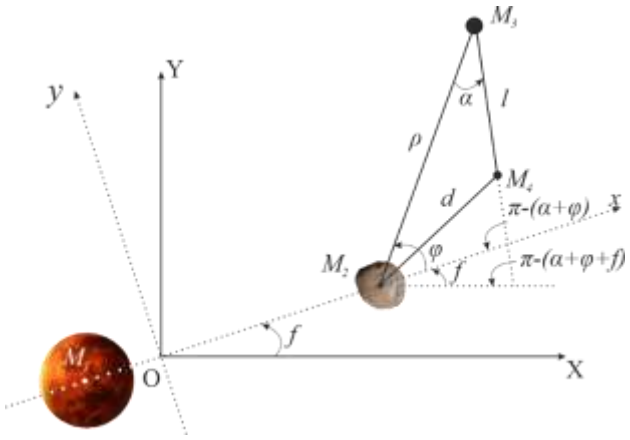

Fig. 1 The frame Oxy and the polar frames ρ,φ and l,α .

A. Key Assumptions

The following assumptions are to be made:

1) Mass of the tether's instrument unit m_4 is supposed to be much smaller than m_3 – the mass of the spacecraft, while m_3 is assumed to be negligible compared with masses m_1 and m_2 of the primary bodies (Mars-Phobos)

$$m_4 \ll m_3 \ll m_2 < m_1 \tag{1}$$

2) It is supposed that the tether is a weightless and rigid rod.

3) The gravitational influence of the end-mass m_4 and the spacecraft m_3 on each other and the primaries are not taken into account. An accuracy of this assumption is confirmed by the restricted three-body problem formulation and the fact that masses m_3, m_4 are insignificant compared with masses of the primaries [28, 29].

B. Equations of motion of the main spacecraft and tether's end-mass in polar coordinates

In the Local-Vertical-Local-Horizontal frame Oxy (Fig. 1) the motion of the spacecraft and the instrument unit is determined by the differential equations of the elliptic restricted three-body problem [28]:

$$\ddot{x}_3 = \frac{\partial W}{\partial x_3} + 2\dot{f}\dot{y}_3 + \ddot{f}y_3 + \dot{f}^2 x_3 \tag{2}$$

$$\ddot{y}_3 = \frac{\partial W}{\partial y_3} - 2\dot{f}\dot{x}_3 - \ddot{f}x_3 + \dot{f}^2 y_3 \tag{3}$$

$$\ddot{x}_4 = \frac{\partial w}{\partial x_4} + 2\dot{f}\dot{y}_4 + \ddot{f}y_4 + \dot{f}^2 x_4 - \frac{1}{m_4}T_x \tag{4}$$

$$\ddot{y}_4 = \frac{\partial w}{\partial y_4} - 2\dot{f}\dot{x}_4 - \ddot{f}x_4 + \dot{f}^2 y_4 - \frac{1}{m_4}T_y \tag{5}$$

where f is true anomaly of the orbit of Phobos, $\vec{T} = (T_x, T_y)$ is the tether tension force, W and w are potential of Eqs. (2)-(5)

$$W(x_3, y_3) = G(\frac{m_1}{R_1} + \frac{m_2}{R_2}) \tag{6}$$

$$w(x_4, y_4) = G(\frac{m_1}{r_1} + \frac{m_2}{r_2}) \tag{7}$$

where G is Newtonian gravitational constant, R_1 is the distance between the primary body 1 and the spacecraft

$$R_1 = \sqrt{(x_3 + r\mu)^2 + y_3^2} \tag{8}$$

R_2 is the distance between the primary body 2 and the spacecraft

$$R_2 = \sqrt{(x_3 - r\nu)^2 + y_3^2} \tag{9}$$

Similarly, r_1 and r_2 respectively are distances between the primaries and the instrument unit

$$r_1 = \sqrt{(x_4 + r\mu)^2 + y_4^2} \tag{10}$$

$$r_2 = \sqrt{(x_4 - r\nu)^2 + y_4^2} \tag{11}$$

where $\nu = \frac{m_1}{m_1 + m_2} = 1 - \mu$, $\mu = \frac{m_2}{m_1 + m_2}$ is the mass ratio, $r = \frac{p}{k}$ is the distance between two primaries, $k = 1 + e\cos f$, $p = a(1 - e^2)$ is a semilatus rectum.

Despite the fact that in this paper the impact of the Phobos terrain is under consideration, the gravitational model is still suggested as in Eqs. (6), (7). Primarily, this is due to the discussion of the planar three-body problem. Of course, when examining the three-dimensional problem, it is necessary to apply models that take into account the non-spherical gravity field of Phobos, as in [30]. Furthermore, it may be necessary not only to take into account the influence of the second zonal harmonic but also the influence of high-order non-spherical gravitational terms [31, 32]. For the closure of the system (1) – (4) we need to enter the expression that describes the dependency between the true anomaly and the time. As the conservation of the angular momentum *c* is valid, the following expression may be written [29]:

$$\dot{f} = \frac{c}{r^2} \tag{12}$$

Now let us make the transition from the Cartesian coordinates to the polar coordinates. The Cartesian coordinates of the spacecraft and the instrument unit in polar reference frames (ρ, φ) and (l, α) can be written as:

$$x_3 = r\nu + \rho\cos\varphi\,, \qquad y_3 = \rho\sin\varphi\,, \tag{13}$$

$$x_4 = r\nu + \rho\cos\varphi - l\cos(\alpha+\varphi), \quad y_4 = \rho\sin\varphi - l\sin(\alpha+\varphi) \tag{14}$$

Describing motion with the polar coordinates allows us to simplify the understanding of the describing processes from a physical point of view. Moreover, it is not so complicated to set the initial conditions for the numerical solution of the equations in the polar coordinate system.

So, Eqs. (2) – (5) take the following form in the polar coordinates (ρ,φ) and (l,α)

$$\rho\dot{\omega} = -\frac{r\nu\dot{f}^2}{k^2}(2ek\cos f\sin\varphi + (k-2e^2\sin f)\sin\varphi) + \frac{r\nu\ddot{f}}{k}(e\sin f\sin\varphi - k\cos\varphi) - 2\dot{\rho}\omega + \frac{Gm_1 r\sin\varphi}{R_1^3} \tag{15}$$

$$\ddot{\rho} = \frac{r\nu\dot{f}^2}{k^2}((k-2e^2\sin f)\cos\varphi - 2ek\sin f\sin\varphi) - \frac{r\nu\ddot{f}}{k}(e\sin f\cos\varphi + k\sin\varphi)$$

$$+\rho\omega^2 - \frac{Gm_1(r\cos\varphi+\rho)}{R_1^3} - \frac{Gm_2}{R_2^2} \tag{16}$$

$$\ddot{l} = \ddot{\rho}\cos\alpha + 2\dot{\rho}\omega\sin\alpha + \rho\dot{\omega}\sin\alpha - \frac{r\nu\dot{f}^2}{k^2}((k^2 - ek\cos f - 2e^2\sin^2 f)\cos\gamma - 2ek\sin f\sin\gamma)$$

$$+l\dot{\theta}^2\sin^2\gamma + \frac{r\nu\ddot{f}}{k}(k\sin\gamma + e\cos\gamma\sin f) + l(\dot{\gamma}^2 + (\dot{\gamma}+\dot{\theta})\dot{f})\cos^2\gamma + \frac{Gm_1(\rho\cos\alpha - l)}{r_1^3}$$

$$+\frac{Gm_2(r\cos\gamma - l + \rho\cos\alpha)}{r_2^3} - \frac{1}{m_4}T \tag{17}$$

$$l\ddot{\theta} = -\frac{r\nu\dot{f}^2}{k^2}((k^2 - ek\cos f - 2e^2\sin^2 f)\sin\gamma + 2ek\sin f\cos\gamma) + 2\dot{l}\dot{\theta} - 2\dot{\rho}\omega\cos\alpha - \rho(\omega^2\sin\alpha + \dot{\omega}\cos\alpha)$$

$$+\ddot{\rho}\sin\alpha - \frac{r\nu\ddot{f}}{k}(k\cos\gamma - e\sin f\sin\gamma) - \frac{Gm_1(r\sin\gamma + \rho\sin\alpha)}{r_1^3} - \frac{Gm_2\rho\sin\alpha}{r_2^3} \tag{18}$$

where

$$R_1 = \sqrt{r^2 + 2\rho r\cos\varphi + \rho^2}, \quad R_2 = \rho \tag{19}$$

$$r_1 = \sqrt{r^2 + 2r(\rho\cos\varphi - l\cos\gamma) + d^2}, \quad r_2 = d \tag{20}$$

$$\gamma = \alpha + \varphi, \quad \omega = \dot{\varphi} + \dot{f}, \quad \dot{\theta} = \dot{\alpha} + \dot{\varphi} + \dot{f} \tag{21}$$

So, the resulting Eqs. (15)–(18) describe the motion of the spacecraft and the instrument unit in polar coordinates (ρ,φ) and (l,α). It is worth noting that for $e=0$, the Eqs. (15)-(18) are reduced to the corresponding Eqs. (14)-(17) in [27] which indicates their correctness.

C. Topographic model of Phobos

The terrain of Phobos is difficult and rough. Its surface has lots of craters of different depths. The largest of them is the Stickney crater [33-36]. In the case of designing a mission to Phobos, it is essential to take into account the topography of Phobos. At least to avoid the collision of the instrument unit with the Phobos surface. The following describes the construction of a 2D cross-section of Phobos. A flat model of Phobos is considered here due to the corresponding problem statement. In considering consideration of the three-dimensional case, it will be necessary to build a 3D model of Phobos. It is proposed to consider the cross-section of Phobos with the OXY plane to build an analytical model of the surface. Then 40 points located on the line of intersection of the secant plane and the Phobos surface are selected. These points are approximated using a Fourier series. Their coefficients are selected so as to make the approximation of the obtained curve and the Phobos model as accurate as possible. For comparison purposes, we will use the Phobos model proposed in [30]. The equation of the curve in the polar frame is written as:

$$R(\psi) = \begin{cases} \sum_{k=1}^{n} R_k \cos(b_1 k\psi - \psi_k), & if\ \ \psi \in [0,\pi] \\ \sum_{i=1}^{n} R_i \cos(b_2 i\psi - \psi_i), & if\ \ \psi \in [\pi,2\pi] \end{cases} \tag{22}$$

where $n = 20$ is number of points in each half-plane. Coefficients b_1 and b_2 are taken as follows:

$$b_1 = 0.408, \quad b_2 = 0.251 \tag{23}$$

$(R_k, \psi_k),\ (R_i, \psi_i)$ are the Fourier series coefficient and the phase shift, presented in Table 1 and Table 2. Values $(R_k, \psi_k),\ (R_i, \psi_i),\ b_1,\ b_2$ are selected to satisfy the criteria of maximal approximation of the model [30] and the curve obtained according to Eq. (22).

Table 1 Fourier series coefficient and phase shift for $\psi \in [0,\pi]$

k	R_k, m	ψ_k, rad
1	5452.41	27.798
2	3004.99	11.655
3	4024.95	23.669
4	2897.45	10.808
5	2155.17	36.973
6	1286.45	95.104
7	780.147	57.817
8	1012.92	-44.180
9	733.64	156.028
10	1404.45	182.038
11	1529.07	23.995
12	1336.58	27.016
13	914.219	7.245
14	417.706	19.779
15	73.090	665.412
16	598.468	-0.611
17	930.446	-12.170
18	998.589	2.536
19	1008.20	-11.215
20	834.348	53.990

Table 2 Fourier series coefficient and phase shift for $\psi \in [\pi, 2\pi]$

i	R_i, m	ψ_i, rad
1	7410.01	17.261
2	5427.83	2.477
3	2543.88	-6.015
4	778.512	13.382
5	2081.15	69.624
6	2950.74	42.179
7	1438.32	8.389
8	1963.24	-20.976
9	845.626	-11.860
10	873.052	37.391
11	1902.98	61.106
12	1284.96	-69.526
13	1618.10	-52.593
14	938.805	25.243
15	-83.643	335.494
16	1147.38	0.471
17	1229.99	57.028
18	1092.90	14.624
19	867.78	10.181
20	294.068	-15.020

Fig. 2 illustrates the combining of the obtained curve and the model of the Phobos surface [30]. It is assumed that for the first attempt the accuracy of the curve is sufficient for modelling the Phobos topography. Note that in paper [27] the cross section of the Phobos surface was approximated only by an ellipse.

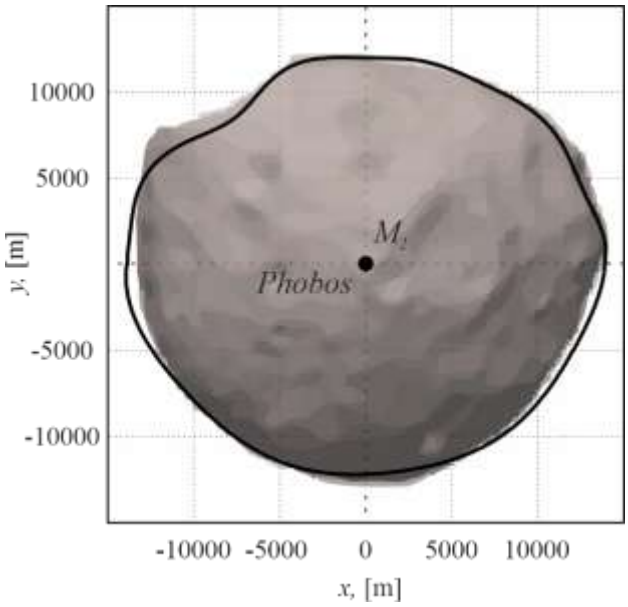

Fig.2 The model of the Phobos surface

The approximation of the Phobos surface by the high-dimensional curve allows to refine the model and make it closer to the real Phobos terrain. Such an approach promotes more precise selection of the control law and the start points for the motion.

III. Deployment of tether system from main spacecraft in low QSO

This section discusses the possibility of studying the Phobos surface from the instrument unit connected to the spacecraft by the tether. The cases where the spacecraft is in four low quasi-satellite orbits (QSOs-L) [37] of different altitudes are considered. The choice of the tether length control law is carried out and the results of this choice are illustrated by means of numerical modeling of the equations of motion.

A. Linear feedback control law

The instrument unit attached to the tether should go around Phobos to explore the surface. As it is shown in [27], this purpose can be achieved by controlling the tether tension force. So, it is proposed to use the feedback control law discussed in [27] for new conditions. It will be discussed below if such a law is effective. Thus, the control law can be written as:

$$T = \begin{cases} k_d(d - R(\psi) - h) + k_v \dfrac{d}{dt} d, & if: \ d - R(\psi) - h < 0 \\ 0, & if: \ d - R(\psi) - h > 0 \end{cases} \tag{24}$$

where *R* is the distance between the center of Phobos and the observation point on its surface, *h* is the altitude where the instrument unit is located, it's supposed fixed and known, k_v and k_d is feedback control law coefficients:

$$k_d = 10 \text{ N m}^{-1} \text{ [N/m]}, \quad k_v = 200 \text{ N s m}^{-1} \text{ [N s/m]} \tag{25}$$

B. Numerical modeling

Under consideration are four QSOs-L, three of which were introduced by Nakamura et al. [37]. QSO (or QRO – distant retrograde orbit) is a trajectory of the spacecraft which located beyond the smaller gravitating body's Hill sphere. Altitudes of QSOs are specified in Table 3, and Fig. 3 presents selected QSOs around Phobos and their evolution during the 24 hours.

Table 3 Size of QSOs-L

QSO	Size
QSO-LA	30 km × 49 km
QSO-LB	22 km × 31 km
QSO-LC	20 km × 27 km
QSO-LD	16 km × 19 km

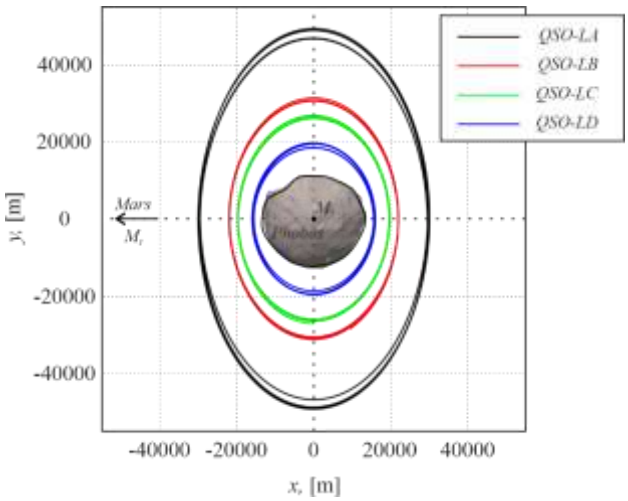

Fig. 3 QSOs-L and their evolution in 24 hours

It is assumed that the start of deployment is at one of two points: $\varphi_{01} = 0$ – the rightmost position or position A, and $\varphi_{02} = -\frac{\pi}{2}$ – the lower position or position B. The initial conditions of the spacecraft and the instrument unit are presented in Table 4. The control law coefficients were chosen after a series of numerical experiments. In some cases, they allow the instrument unit to make a complete revolution around Phobos. The numerical experiments conducted to select the coefficients that will allow the instrument unit to spend the maximum time at a given altitude above the Phobos surface.

Table 4 Initial conditions and control law coefficients for the tether system deployment

QSO	Starting position	Initial conditions
QSO-LA 30000 m × 49000 m	A	$\rho_{01} = 30000$ m, $\dot{\rho}_{01} = 0$ m s^{-1} [m/s], $\varphi_{01} = 0$ rad, $\dot{\varphi}_{01} = -0.00052$ rad s^{-1} [rad/s], $\alpha_{01} = 0.1$ rad, $\dot{\alpha}_{01} = -0.33$ rad s^{-1} [rad/s], $l_{01} = 1$ m, $\dot{l}_{01} = 0.5$ m s^{-1} [m/s]
	B	$\rho_{02} = 49045$ m, $\dot{\rho}_{02} = -0.063$ m s^{-1} [m/s], $\varphi_{02} = -\frac{\pi}{2}$ rad, $\dot{\varphi}_{02} = -0.00018$ rad s^{-1} [rad/s], $\alpha_{02} = 0.1$ rad, $\dot{\alpha}_{02} = 0$ rad s^{-1} [rad/s], $\rho_{02} = 49045$ m, $\dot{l}_{02} = 5.5$ m s^{-1} [m/s]
QSO-LB 22000 m × 31000 m	A	$\rho_{01} = 22000$ m, $\dot{\rho}_{01} = 0$ m s^{-1} [m/s], $\varphi_{01} = 0$ rad, $\dot{\varphi}_{01} = -0.00059$ rad s^{-1} [rad/s], $\alpha_{01} = 0.1$ rad, $\dot{\alpha}_{01} = -0.33$ rad s^{-1} [rad/s], $l_{01} = 1$ m, $\dot{l}_{01} = 0.5$ m s^{-1} [m/s]

	B	$\rho_{02} = 31200$ m,	$\dot{\rho}_{02} = -0.0324$ m s^{-1} [m/s],
		$\varphi_{02} = -\frac{\pi}{2}$ rad,	$\dot{\varphi}_{02} = -0.00026$ rad s^{-1} [rad/s],
		$\alpha_{02} = 0.1$ rad,	$\dot{\alpha}_{02} = 0$ rad s^{-1} [rad/s],
		$l_{02} = 1$ m,	$\dot{l}_{02} = 4$ m s^{-1} [m/s]
QSO-LC 20000 m × 27000 m	A	$\rho_{01} = 20000$ m,	$\dot{\rho}_{01} = 0$ m s^{-1} [m/s],
		$\varphi_{01} = 0$ rad,	$\dot{\varphi}_{01} = -0.00062$ rad s^{-1} [rad/s],
		$\alpha_{01} = 0.1$ rad,	$\dot{\alpha}_{01} = -0.33$ rad s^{-1} [rad/s],
		$l_{01} = 1$ m,	$\dot{l}_{01} = 0.5$ m s^{-1} [m/s]
	B	$\rho_{02} = 27099$ m,	$\dot{\rho}_{02} = -0.0036$ m s^{-1} [m/s],
		$\varphi_{02} = -\frac{\pi}{2}$ rad,	$\dot{\varphi}_{02} = -0.000306$ rad s^{-1} [rad/s],
		$\alpha_{02} = 0.1$ rad,	$\dot{\alpha}_{02} = 0$ rad s^{-1} [rad/s],
		$l_{02} = 1$ m,	$\dot{l}_{02} = 4$ m s^{-1} [m/s]
QSO-LD 16000 m × 19000 m	A	$\rho_{01} = 16000$ m,	$\dot{\rho}_{01} = 0$ m s^{-1} [m/s],
		$\varphi_{01} = 0$ rad,	$\dot{\varphi}_{01} = -0.00072$ rad s^{-1} [rad/s],
		$\alpha_{01} = 0.1$ rad,	$\dot{\alpha}_{01} = -0.33$ rad s^{-1} [rad/s],
		$l_{01} = 1$ m,	$\dot{l}_{01} = 0.5$ m s^{-1} [m/s]
	B	$\rho_{02} = 19634$ m,	$\dot{\rho}_{02} = -0.065$ m s^{-1} [m/s],
		$\varphi_{02} = -\frac{\pi}{2}$ rad,	$\dot{\varphi}_{02} = -0.00044$ rad s^{-1} [rad/s],
		$\alpha_{02} = 0.01$ rad,	$\dot{\alpha}_{02} = 0.1$ rad s^{-1} [rad/s],
		$l_{02} = 1$ m,	$\dot{l}_{02} = 1.1$ m s^{-1} [m/s]

Figs. 4 – 5 show the deployment of the tether system from the first lower and the rightmost positions, respectively. According to Fig.4, the instrument unit flies away from the Phobos surface in case of deployment liftoff from the lower position of the QSO-LD, while the deployment of the tether system from the rightmost position of the QSO-LD causes the collision of the instrument unit and Phobos, as shown in Fig. 5.

The cases when the main spacecraft locates in the orbits of A, B, C types are being discussed. When the deployment of the tether system starts from the higher altitudes, the instrument unit does not perform a complete revolution around Phobos again (Figs. 6 – 11). When the deployment begins from position B of the selected orbits the instrument unit collides with Phobos. In other cases, the results of numerical modelling show that the instrument unit does not achieve the set altitude above the Phobos surface, it stays much higher, and its trajectory is close to the main spacecraft orbit.

All in all, the trajectories of the instrument unit are qualitatively similar for the deployment from the QSO-LC, LB, LA. Under the action of the control law presented in Eq. (24) the instrument unit does not reach the required altitude above Phobos or crashes into it.

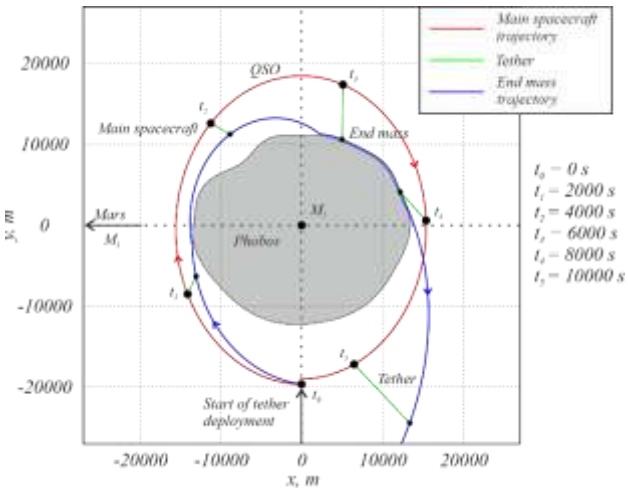

Fig. 4 Deployment of the tether system, starting at the moment when the main spacecraft is at the lower point of QSO-LD.

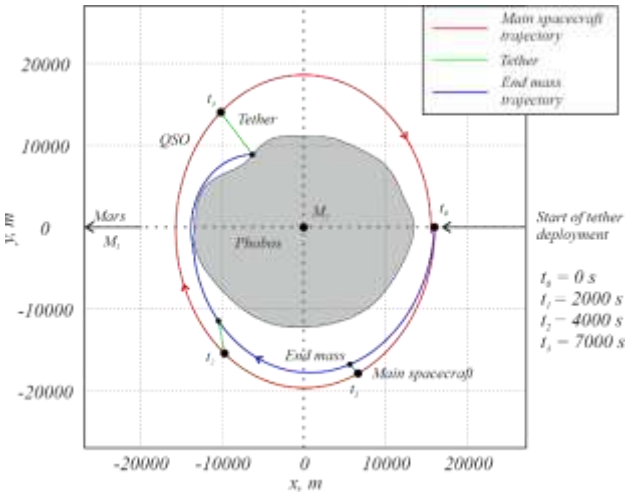

Fig. 5 Deployment of the tether system, starting at the moment when the main spacecraft is at the rightmost point of QSO-LD.

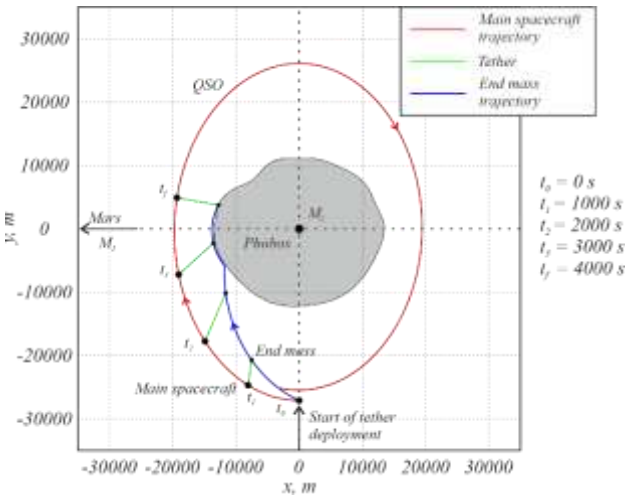

Fig. 6 Deployment of the tether system, starting at the moment when the main spacecraft is at the lower point of QSO-LC.

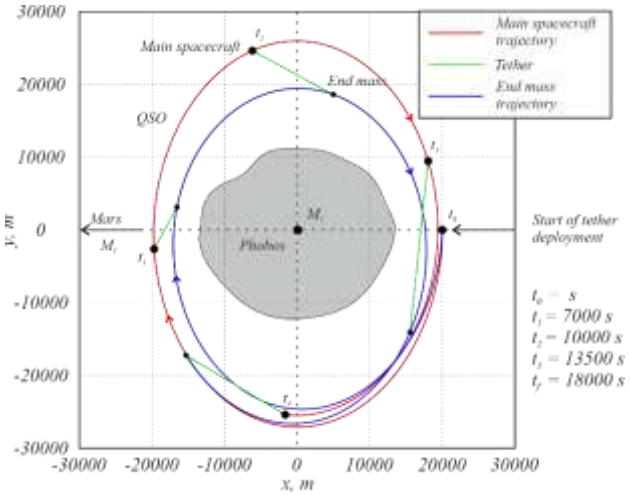

Fig. 7 Deployment of the tether system, starting at the moment when the main spacecraft is at the rightmost point of QSO-LC

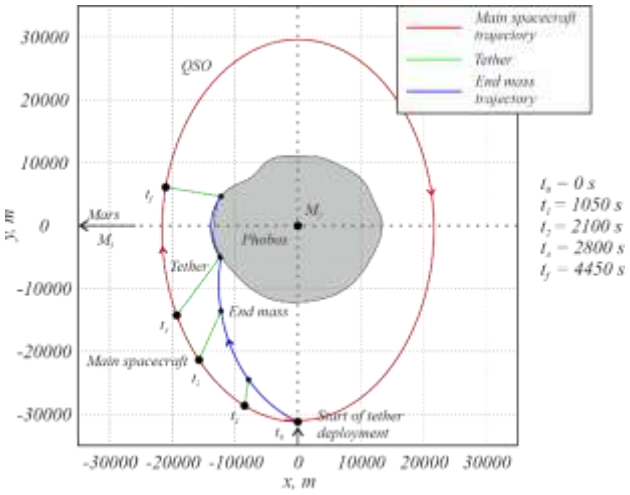

Fig. 8 Deployment of the tether system, starting at the moment when the main spacecraft is at the lower point of QSO-LB.

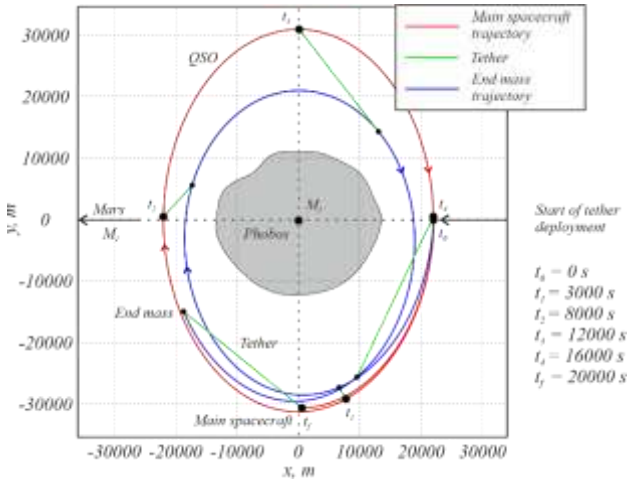

Fig. 9 Deployment of the tether system, starting at the moment when the main spacecraft is at the rightmost point of QSO-LB.

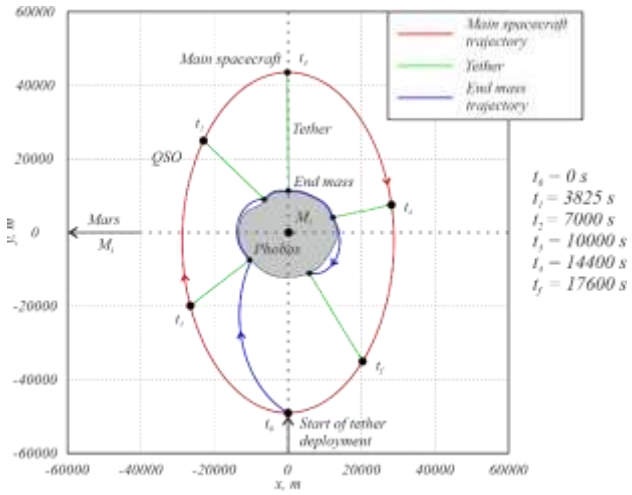

Fig. 10 Deployment of the tether system, starting at the moment when the main spacecraft is at the lower point of QSO-LA.

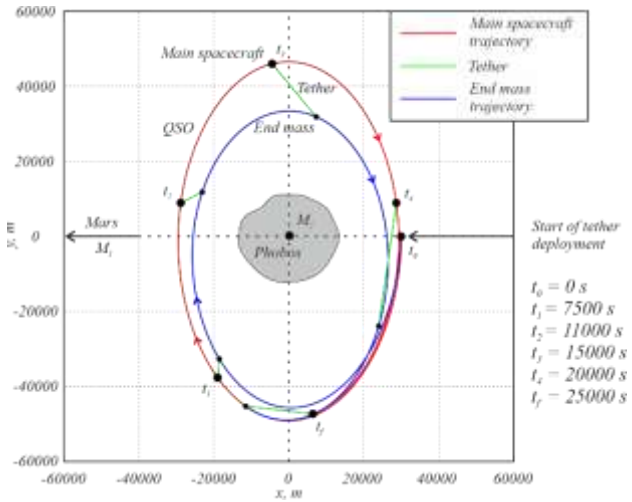

Fig. 11 Deployment of the tether system, starting at the moment when the main spacecraft is at the rightmost point of QSO-LA.

In summary, Figs. 6 – 11 do not present the desired trajectory of the instrument unit motion under the action of the linear control law introduced in Eq. (24). The instrument unit does not perform the complete revolution around Phobos in all cases of the tether deployment.

C. Nonlinear feedback control law

It is possible to extend the scope of the feedback control law by adding a quadratic term to the law in Eq. (24). So, the new feedback control law can be written as:

$$T = \begin{cases} k_d(d - R - h) + k_v \dfrac{d}{dt} d + k_s \left(\dfrac{d}{dt} d \right)^2, & if: \ d - R - h < 0 \\ 0, & if: \ d - R - h > 0 \end{cases} \tag{26}$$

where k_s is the additional coefficient for the quadratic term.

The effect of the control law presented in Eq. (26) on the motion of the instrument unit is studied for the four QSOs considered previously. The start of the deployment are the same points: the rightmost position $\varphi_{01} = 0$ and the lower position $\varphi_{02} = -\dfrac{\pi}{2}$. The initial conditions are suggested to be the same and can be found in Table 4. The control law coefficients for each orbit are presented in Table 5. As in the case of the linear control law, these coefficients had been chosen in order to make the instrument unit move at the set altitude around Phobos. When the real missions are planned, such values should be selected to meet the technical specifications of the equipment or to satisfy necessary criteria. For example, to maintain the value of the required speed of the motion or the tension force of the tether.

Table 5 Nonlinear control law coefficients

QSO	Control law coefficients
QSO-LA 30000 m × 49000 m	$k_d = 10$ N m^{-1} [N/m], $k_v = 245$ N s m^{-1} [N s/m], $k_s = -40$ N s^2 m^{-1} [N s^2/m]
QSO-LB 22000 m × 31000 m	$k_d = 10$ N m^{-1} [N/m], $k_v = 245$ N s m^{-1} [N s/m], $k_s = -40$ N s^2 m^{-1} [N s^2/m]
QSO-LC 20000 m × 27000 m	$k_d = 10$ N m^{-1} [N/m], $k_v = 200$ N s m^{-1} [N s/m], $k_s = -40$ N s^2 m^{-1} [N s^2/m]

QSO-LD 16000 m × 19000 m	$k_d = 10$ N m^{-1} [N/m], $k_v = 250$ N s m^{-1} [N s/m], $k_s = -50$ N s^2 m^{-1} [N s^2/m]

Figs. 12 – 19 show the deployment of the tether system from the lower and rightmost points of each orbit that is under consideration. In all cases, when the deployment of the tether starts from the lower position, the instrument unit under the action of the control law presented in Eq.(26) performs the complete revolution around Phobos. In addition, launching the deployment of the tether system from the opposite point ($\varphi_{02} = -\frac{3\pi}{2}$) gives us the similar result.

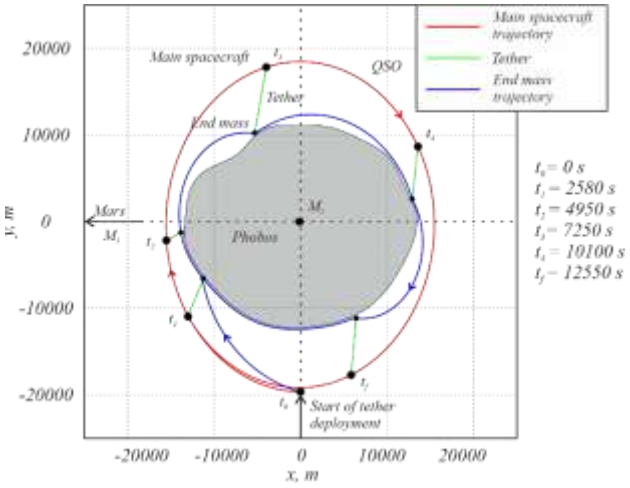

(a) Deployment of the tether system from the lower point of under the acting of the nonlinear control law

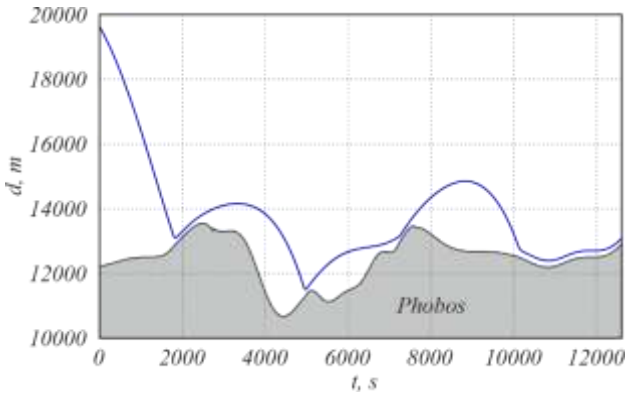

(b) The instrument unit flight trajectory above the Phobos surface

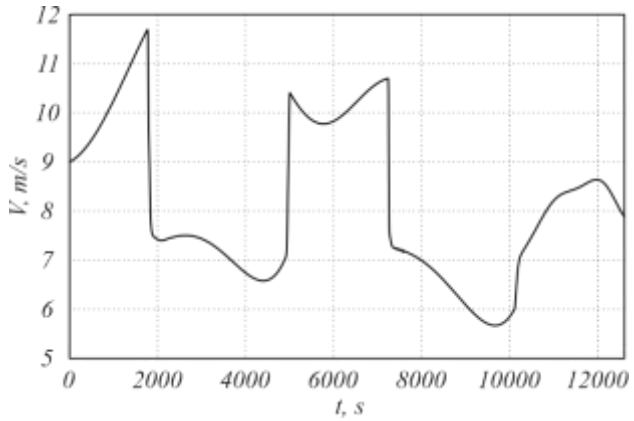

(c) The instrument unit flight velocity

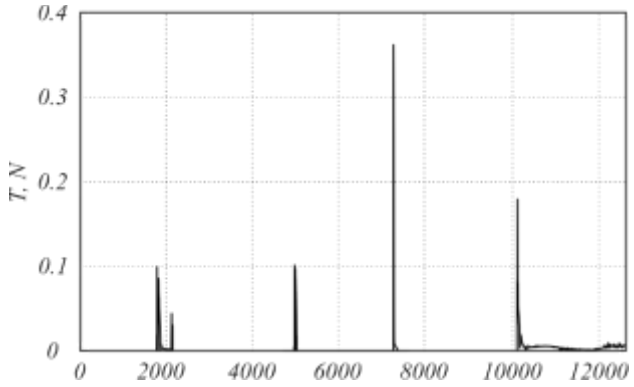

(d) Time history the tension force under the impact of the control law

Fig.12 The main spacecraft locates at the lower point of the QSO-LD.

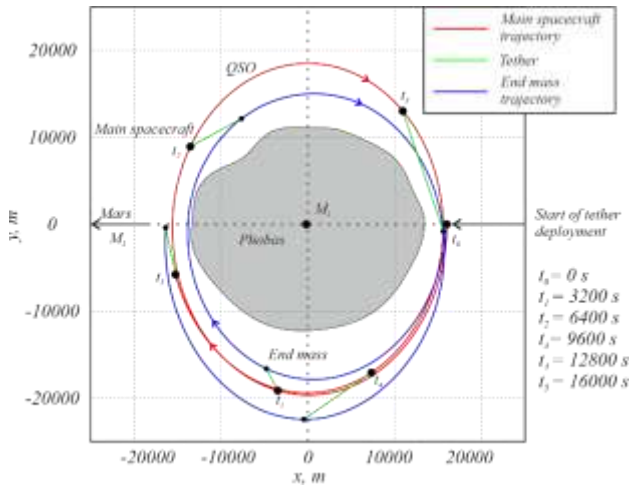

Fig. 13 Deployment of the tether system from the rightmost point of QSO-LD under the acting of the nonlinear control law.

So, the numerical modeling shows that the quadratic term addition to the control law leads to an increase in the number of possible deployment start points. Fig. 12(c) demonstrates that the maximum instrument unit velocity is

achieved when the instrument unit starts its revolution around Phobos. The oscillations in the velocity value are rather small during the instrument unit flight above Phobos surface.

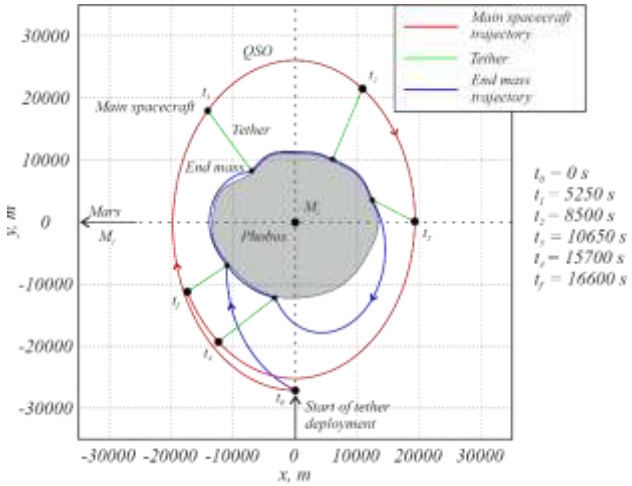

(a) Deployment of the tether system from the lower point under the acting of the nonlinear control law

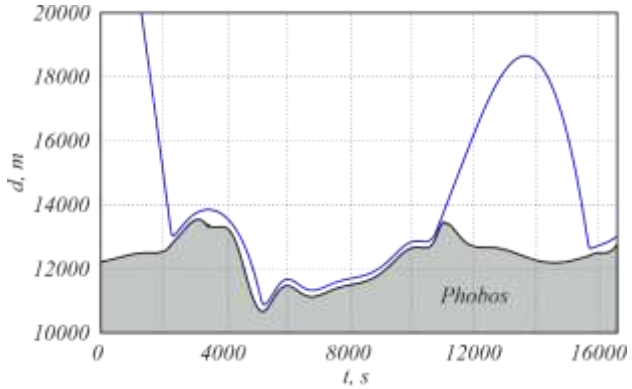

(b) The instrument unit flight trajectory above the Phobos surface

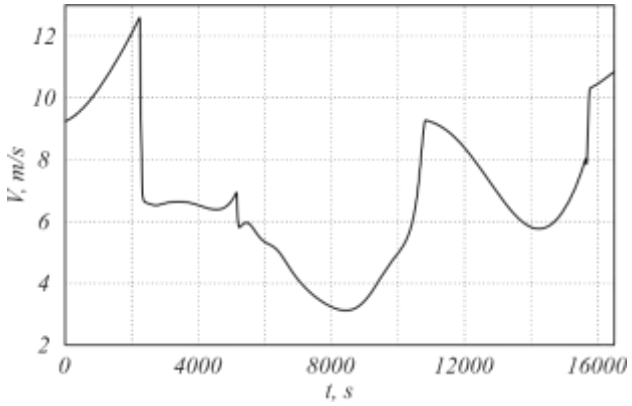

(c) The instrument unit flight velocity

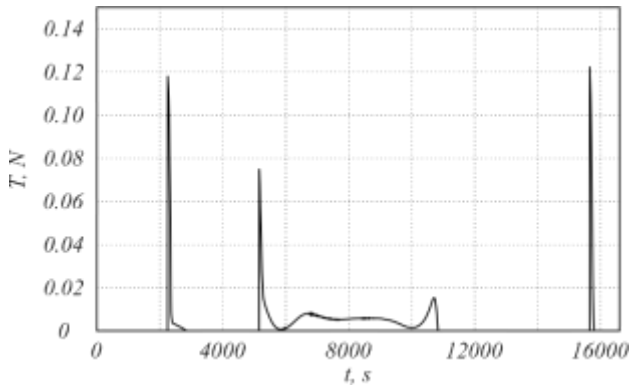

(d) Time history the tension force under the impact of the control law

Fig.14 The main spacecraft locates at the lower point of the QSO-LC.

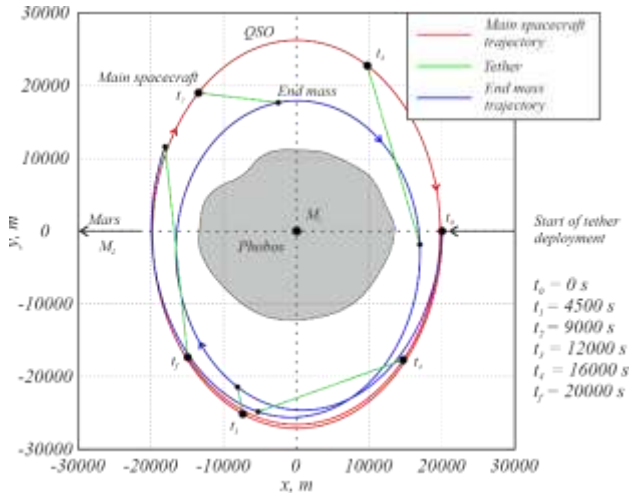

Fig. 15 Deployment of the tether system from the rightmost point of QSO-LC under the acting of the nonlinear control law.

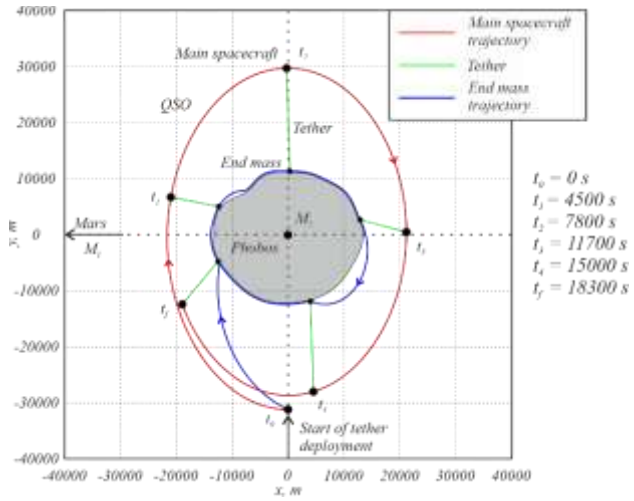

(a) Deployment of the tether system from lower point under the acting of the nonlinear control law

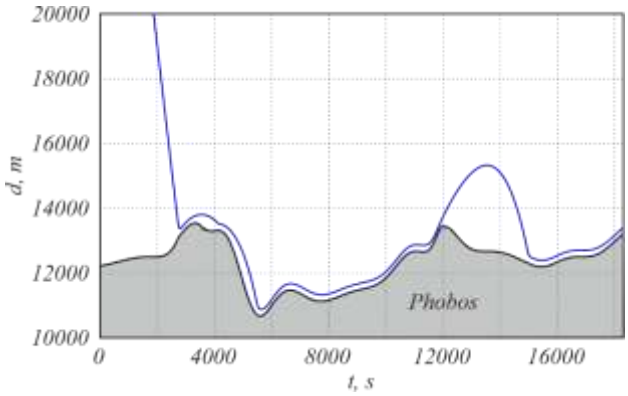

(b) The instrument unit flight trajectory above the Phobos surface

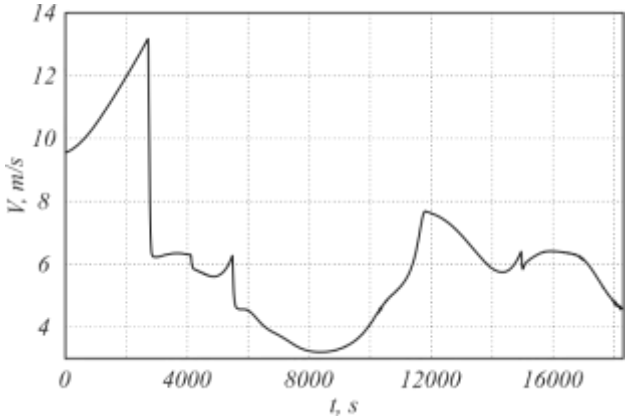

(c) The instrument unit flight velocity

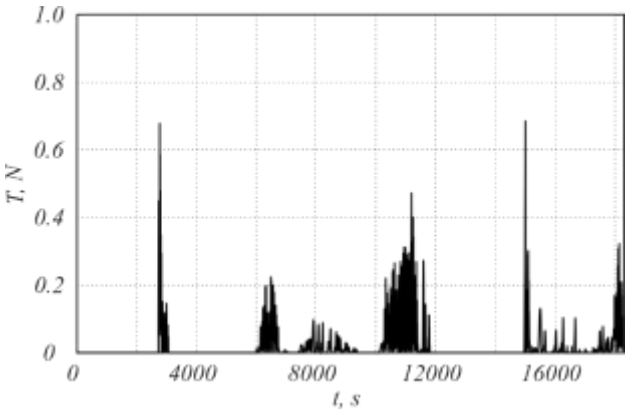

(d) Time history the tension force under the impact of the control law

Fig.16 The main spacecraft locates at the lower point of the QSO-LB.

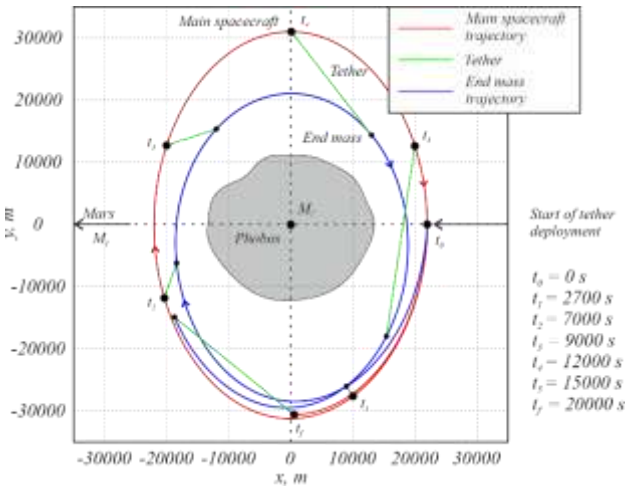

Fig. 17 Deployment of the tether system from the rightmost point of QSO-LB under the acting of the nonlinear control law.

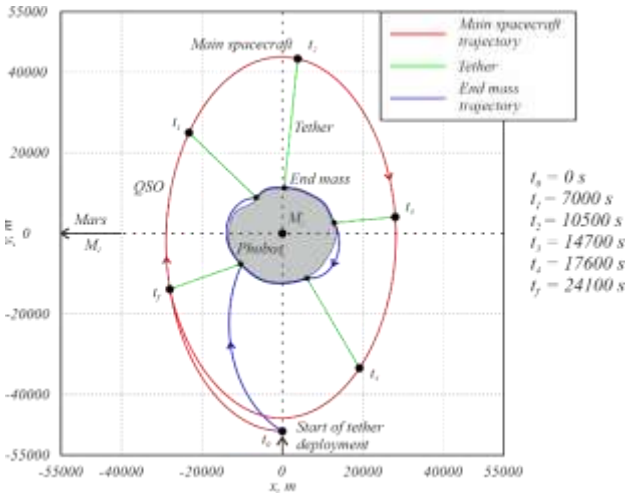

(a) Deployment of the tether system from the lower point under the acting of the nonlinear control law

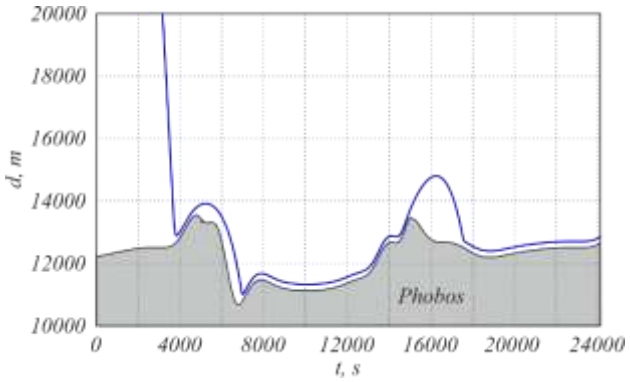

(b) The instrument unit flight trajectory above the Phobos surface

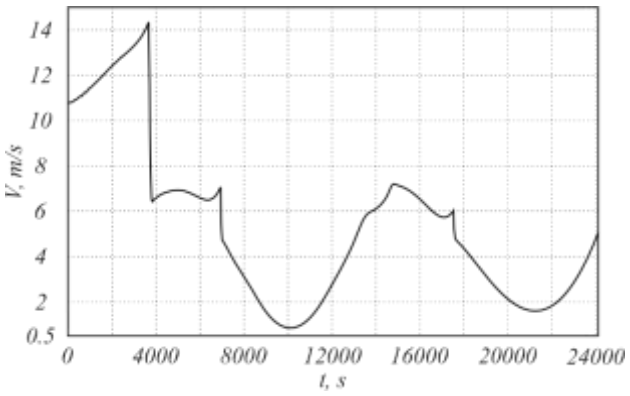

(c) The instrument unit flight velocity

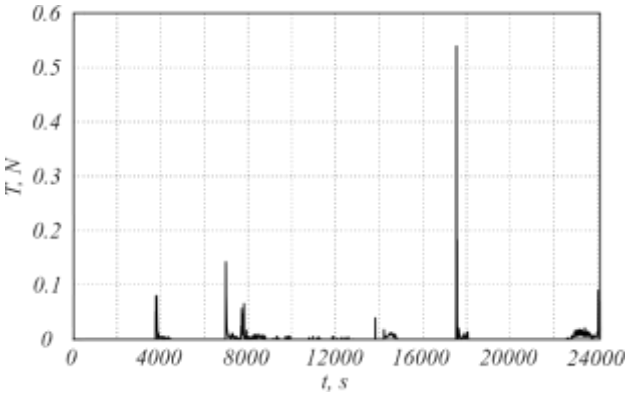

(d) Time history the tension force under the impact of the control law

Fig.18 The main spacecraft locates at the lower point of the QSO-LA.

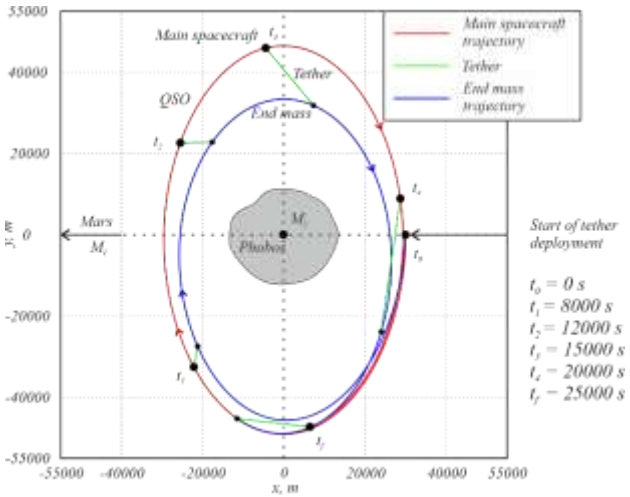

Fig. 19 Deployment of the tether system from the rightmost point of QSO-LA under the acting of the nonlinear control law.

As opposed to the linear control law presented in Eq.(24), the nonlinear feedback control law introduced in Eq.(26) allows expanding the number of start points for the tether deployment. Specifically, to add the lower points of all selected QSOs. So, the quadratic term of the nonlinear control law affords offsetting the impact of the eccentricity of Phobos orbit and the approximation curve for the Phobos surface, it's shown by Figs. 12, 14, 16, 18 (a). For the

rightmost points, the trajectories of the instrument unit under the action of the control laws presented in Eqs.(24), (26) are qualitatively similar (Figs. 5 – 11, Figs. 13 – 19).

It is worth specifying that the time necessary for the tether deployment and the complete revolution around Phobos is in the interval from 12550 s to 24100 s depending on the altitude where the spacecraft is located. Figs. 12, 14, 16, 18 (c) illustrate the instrument unit velocity, which does not exceed the value of 14.2 m/s. The tension force acting on the instrument unit does not surpass the value of 0.7 N (Figs. 12, 14, 16, 18 (d)). It is worth noting that the control law presented in Eq. 26 starts acting only under the conditions introduced in Eq. 26, which is also reflected in Figs. 12, 14, 16, 18 (d). Also orbits of A and B types are the best to start the tether deployment because in these cases the instrument unit will diverge less from the target distance.

IV. Retrieval of the tether system

In this section the possibility of delivering the instrument unit back to the spacecraft by the tether system retracting is being discussed. The method of minimizing the tether oscillation during the retraction is illustrated. The control law that reduces the oscillation based on the tether angular attitude control is presented.

As it was shown in [27], the fastest retraction can be achieved by the tether retracting at a constant velocity. So, suppose the tether is retracted at a constant velocity (V_r):

$$\dot{l} = -V_r \text{ m s}^{-1} \text{ [m/s]}, \quad \ddot{l} = 0 \text{ m s}^{-2} \text{ [m/s}^2\text{]} \tag{27}$$

Then the length of the tether is changed as follows:

$$l = L - V_r t \tag{28}$$

where L is the tether length at the beginning of the retraction.

The tether system retraction is describing by Eqs. (15) - (18) taking into account Eqs. (27) - (28). Clearly, the instrument unit motion is determined by Eq. (28) and the following equation:

$$\begin{aligned} l\ddot{\alpha} = {} & (\ddot{\rho} - \rho\dot{f}^2 - \rho\dot{\varphi}^2 - 2\rho\dot{\varphi}\dot{f})\frac{\sin\varphi}{\sin\gamma} + (2\dot{\rho}\dot{\varphi} + 2\dot{\rho}\dot{f} + \rho\ddot{\varphi})\frac{\cos\varphi}{\sin\gamma} + l(\dot{\gamma}^2 + \dot{f}^2 + 2\dot{f}\dot{\gamma}) + 2e\dot{f}^2\frac{r\nu}{k}\frac{\sin f}{\sin\gamma} + \\ & (r\nu - l\cos\gamma + \rho\cos\varphi)\frac{\ddot{f}}{\sin\gamma} - l\ddot{\varphi}\cot\gamma - 2V_r(\dot{\gamma} + \dot{f})\cot\gamma + G(\frac{\rho\sin\varphi}{\sin\gamma} - l)(\frac{m_1}{r_1^3} + \frac{m_2}{r_2^3}) \end{aligned} \tag{29}$$

Start of the retraction is considered to be from the point of the deployment finish. The point corresponding to the end of the instrument unit's trajectory around Phobos is as follows:

$$\begin{aligned} &\rho_0 = 17001 \text{ m}, \quad \dot{\rho}_0 = -1.81 \text{ m s}^{-1} \text{ [m/s]}, \\ &\varphi_0 = -8.72 \text{ rad}, \dot{\varphi}_0 = -00060 \text{ rad s}^{-1} \text{ [rad/s]}, \\ &\alpha_0 = 0.49 \text{ rad}, \quad \dot{\alpha}_0 = 0.00035 \text{ rad s}^{-1} \text{ [rad/s]}, \\ &\nu_0 = 2.87 \text{ rad}, \quad \dot{\nu}_0 = 0.00022 \text{ rad s}^{-1} \text{ [rad/s]} \end{aligned} \tag{30}$$

Eq. (30) is the end condition of the tether deployment from the rightmost position of the QSO-LD. And characteristics of the tether system at the start of the retracting are taking as following:

$$L = 4723.5 \text{ m}, \quad V_r = 1.57 \text{ m s}^{-1} \text{ [m/s]} \tag{31}$$

The values presented in Eq. (31) were also found in the numerical simulation. The tether length at the beginning of the retraction L is the tether length at the end of the instrument unit flight. And the velocity of the instrument unit during the retraction is found in such a way that the tension force of the tether remains positive throughout the entire retraction.

Fig. 20 illustrates that in the case of the uniform tether retraction, the instrument unit turns around the spacecraft under the action of the Coriolis force $2m_4V_r(\dot{\gamma}+\dot{f})$, which can be noticed in Eq. (29). Also, this can be explained by the kinetic momentum theorem.

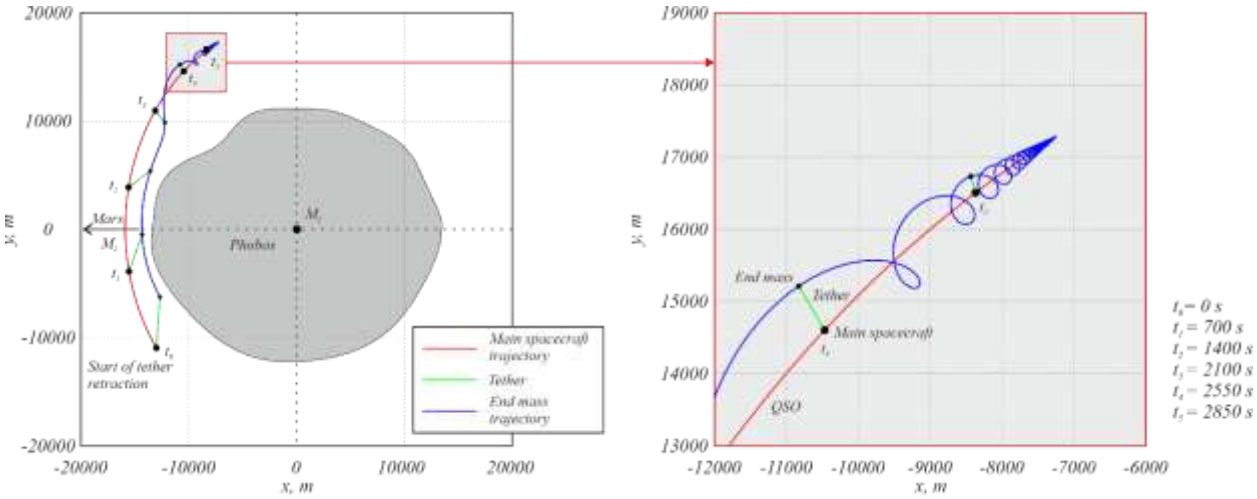

Fig. 20 Retrieval of the tether system.

One of the methods can be used to prevent the instrument unit from turning around the main spacecraft is to set small thrusters on the instrument unit. In that case, feedback control is essential to preclude the oscillation of the tether. We use the control law, similar to the law presented in [27]:

$$u = k_\alpha(\alpha - \alpha_d) + k_\omega \frac{d\alpha}{dt} \tag{32}$$

where k_α and k_ω are the control law coefficients.

The control law coefficients are considered as follows [27]:

$$k_\alpha = 1 \text{ m}^{-1}\text{s}^{-2}, \quad k_\omega = 10 \text{ m}^{-1}\text{s}^{-1} \tag{33}$$

The initial conditions remain the same as in Eq. (30). Fig. 21 illustrates the efficiency of the retrieval control law. It is worth noting that the tension force is positive during all the time of the retraction and its peak value is rather small

– near 0.005 N (Fig. 22). In consideration of the other QSOs-L, the control law coefficients remain the same, while initial conditions should match with the end point of deployment (Figs. 23 – 28).

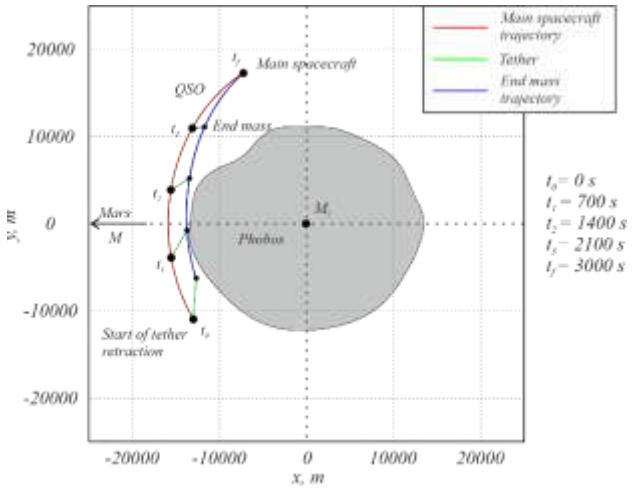

Fig. 21 Retrieval of the tether system under the action of the stabilization control law, when the main spacecraft locates in the QSO-LD.

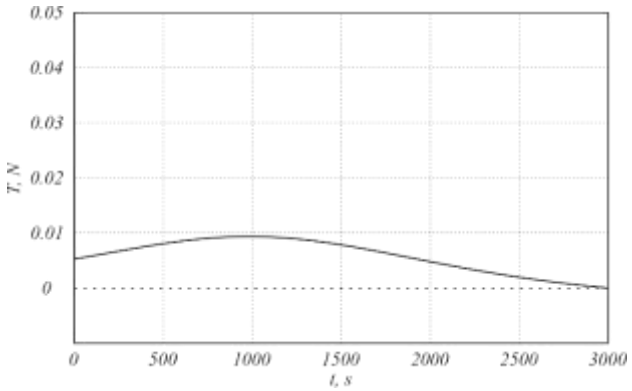

Fig. 22 Time history of the tension force.

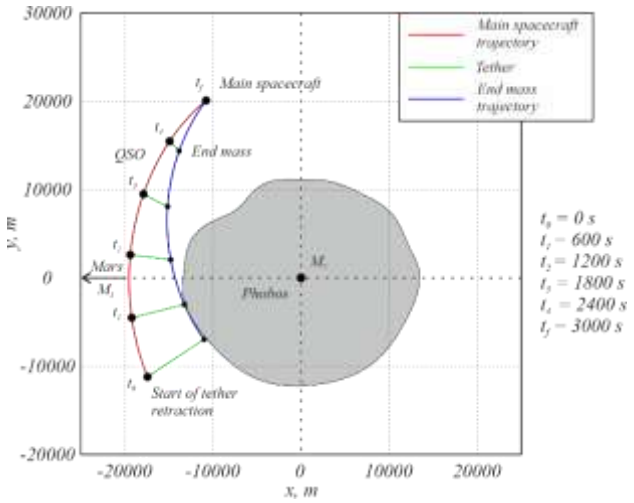

Fig. 23 Retrieval of the tether system under the action of the stabilization control law, when the main spacecraft locates in the QSO-LC.

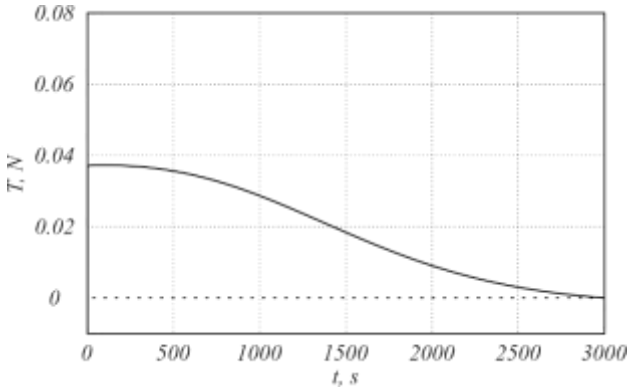

Fig. 24 Time history of the tension force.

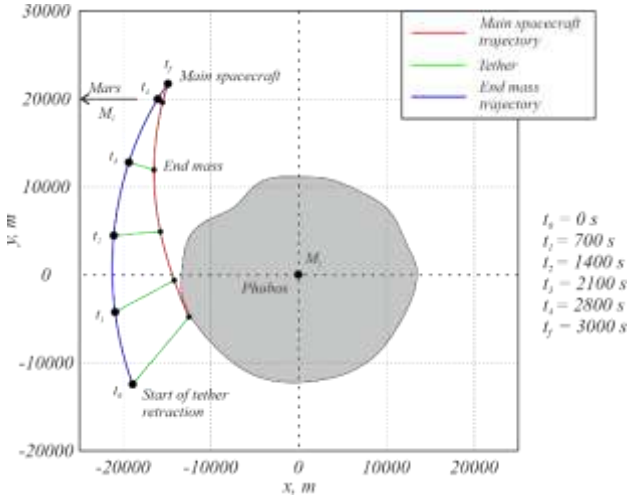

Fig. 25 Retrieval of the tether system under the action of the stabilization control law, when the main spacecraft locates in the QSO-LB.

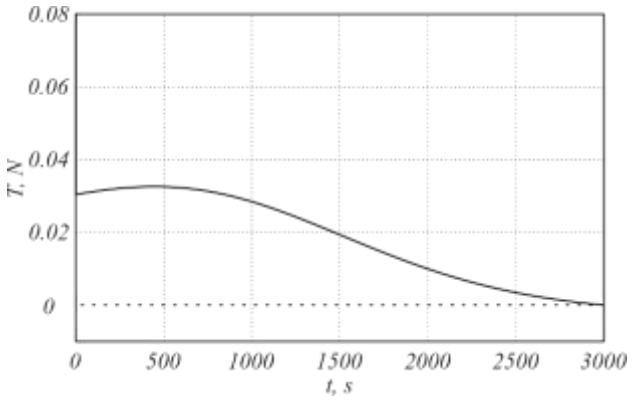

Fig. 26 Time history of the tension force

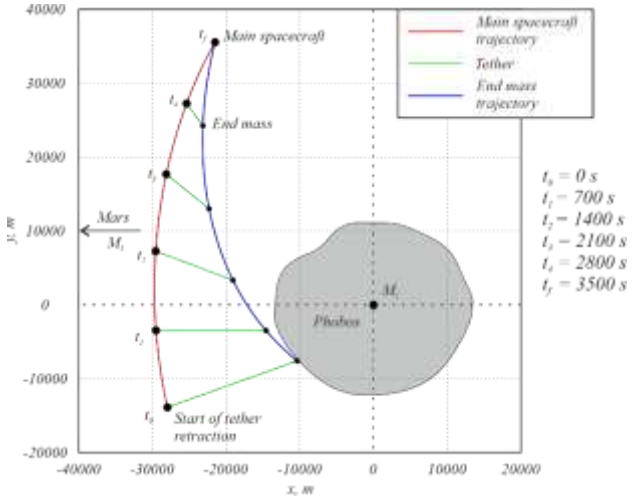

Fig. 27 Retrieval of the tether system under the action of the stabilization control law, when the main spacecraft locates in the QSO-LA.

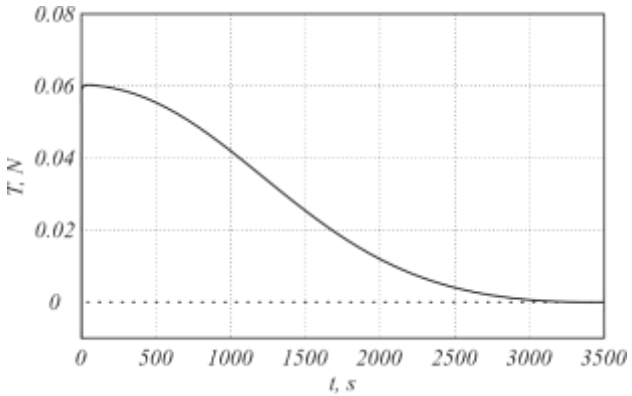

Fig. 28 Time history of the tension force.

As can be seen from Figs. 23–28, the tether retraction is successful under the action of the control law presented in Eq. (32), with the tension force staying small and not exceeding 0.06 N.

V. Conclusions

In this paper, the possibility of the Phobos surface exploration in terms of the elliptic restricted three-body problem with the tether fixed to the spacecraft located in low quasi-satellite orbits is discussed. Both the eccentricity of the Phobos orbit and the topography of Phobos have an impact on the motion of the instrument unit. However, the greater effect has the approximation of the Phobos surface with the curve imitating the Phobos topography. The results of the research can be summarized as follows:

1) The differential equations of the motion of the spacecraft and the instrument unit are derived in the framework of the elliptic restricted three-body problem. Two control laws for operation of the tether system are discussed.

2) The numerical simulation has shown that it takes the instrument unit from 12550 s to 24100 s to reach the altitude of 200 m above the Phobos surface and make the complete revolution around it depending on the orbit altitude. Herewith, maximum instrument unit velocity varies from 11.7 m/s to 14.2 m/s in different orbits, and the value of the tension force is in the interval from 0.12 N to 0.8 N.

3) In case of the retraction of the tether system, it takes the instrument unit near 3500 s to return to the spacecraft. The tether tension force lies in the interval from 0.005 N to 0.06 N depending on the orbit in which the spacecraft is located. In addition, the tension force remains positive under the presented control law in all cases.

The results of this paper can be useful during the development of MMX-like missions or missions focused on the moons of other planets. In the further development the work can be focused on the consideration of the three-dimensional case of the problem and the development of more detailed model of the Phobos topography including the investigation of the influence of more accurate gravitational models of Phobos on the instrument unit motion.

References

[1] Albee, A. L., Palluconi, F.D., Arvidson, R.E., “Mars global surveyor mission: overview and status”, *Science*, Vol. 279, No. 5357, 1998, pp. 1671-1672.
https://doi.org/10.1126/science.279.5357.1671

[2] Zurek, R.W., Smrekar, S.E., “An overview of the Mars Reconnaissance Orbiter (MRO) science mission”, *Journal of Geophysical Research: Planets*, Vol. 112, No. E5, 2007.
http://dx.doi.org/10.1029/2006JE002701

[3] Marov, M.Y., “Phobos-Grunt: Russian sample return mission”, *Advances in Space research*, Vol. 33, No. 12, 2004, pp. 2276-2280.
http://dx.doi.org/10.1016/S0273-1177(03)00515-5

[4] Dobrovolskiy, A.R., Burns, J.A., “Life near the Roche limit: behavior of ejecta from satellites close to planets”, *Icarus,* Vol. 42, No. 3, pp. 422–441. https://doi.org/10.1016/0019-1035(80)90105-0

[5] Wiesel, E. W., “Stable orbits about the martian moons”, *Journal of Guidance, Control and Dynamics,* Vol. 16, No. 3, 1993, pp. 434-440. https://doi.org/10.2514/3.21028

[6] Baresi, N., Dell’Elce, L., Cardoso dos Santos, J., Kawakatsu, Y., “Long-term evolution of mid-altitude quasi-satellite orbits”, *Nonlinear Dynamics,* Vol. 99, 2020, pp. 2743-2763. https://doi.org/10.1007/s11071-019-05344-4

[7] Baresi, N., Dell'Elce, L., Cardoso dos Santos, J., Kawakatsu, Y., “Orbit maintenance of quasi-satellite trajectories via mean relative orbit elements”, *Proceedings of the 69th International Astronautical Congress,* 2018.

[8] Baresi, N., Diogene, A., Dei Tos, Ikeda, H., Kawakatsu, Y., “Trajectory design and maintenance of the Martian Moons eXploration mission around Phobos”, *Journal of Guidance, Control and Dynamics*, Vol. 44, No. 5, 2020, pp. 996-1007. https://doi.org/10.2514/1.G005041

[9] Lara, M., “Design of quasi-satellite orbits: Analytical alternatives”, *International Symposium on Space Flight Dynamics*, 2019, pp. 1674-1685. https://doi/abs/10.3316/informit.326939818512964

[10] Carletta, S., Pontani, M., Teofilatto, P., “Characterization of Low-Energy Quasiperiodic Orbits in the Elliptic Restricted 4-Body Problem with Orbital Resonance”, *Aerospace*, Vol. 9, No. 4, 2022, pp. 175. https://doi.org/10.3390/aerospace9040175

[11] Ershkov, S., Leshchenko, D., Prosviryakov, E. Y., “Semi-analytical approach in BiER4BP for exploring the stable positioning of the elements of a Dyson sphere”, *Symmetry*, Vol. 15, No. 2, 2023, pp. 326. https://doi.org/10.3390/sym15020326

[12] Kuramoto, K., Kawakatsu, Y., Fujimoto, M., Araya, A., Barucci, M.A., Genda, H., Hirata, N., Ikeda, H., Imamura, T., Helbert, J., Kameda, S., “Martian Moons Exploration MMX: Sample Return Mission to Phobos Elucidating Formation Processes of Habitable Planets,” *Earth Planets Space,* Vol. 74, No. 1, 2022, pp. 1–31. https://doi.org/10.1186/s40623-021-01545-7

[13] Beletsky, V. V., Levin, E. V., *Dynamics of Space Tether Systems*, Univelt, San Diego, CA, 1993.

[14] Levin, E. M., *Dynamic Analysis of Space Tether Missions,* Univelt, San Diego, CA, 2007.

[15] Aslanov, V. S., Ledkov, A. S., *Dynamics of Tethered Satellite Systems*, Woodhead Publ., Cambridge, England, U.K., 2012.

[16] Cartmell, M.P., McKenzie, D.J., "A review of space tether research", *Progress in Aerospace sciences*, Vol. 44, No. 1, 2008, pp. 1-21.
https://doi.org/10.1016/j.paerosci.2007.08.002

[17] Huang, P., Zhang, F., Chen, L., Meng, Z., Zhang, Y., Liu, Z., Hu, Y., "A review of space tether in new applications", *Nonlinear Dynamics*, Vol. 94, No.1, 2018, pp.1-19.
https://doi.org/10.1007/s11071-018-4389-5

[18] Aslanov, V.S., "A double pendulum fixed at the L1 libration point: a precursor to a Mars-Phobos space elevator", *Nonlinear Dynamics*, Vol. 112, 2024, pp. 775-791.
https://doi.org/10.1007/s11071-023-09108-z

[19] Aslanov, V.S., Ledkov, A.S., "Swing principle in tether-assisted return mission from an elliptical orbit", *Aerospace Science and Technology*, Vol. 71, 2017, pp. 156-162
https://doi.org/10.1016/j.ast.2017.09.006

[20] Aslanov, V.S., Bilén, S. G., Johnson, L., Sánchez-Arriaga, G., "Tethers in space", *Acta Astronautica*, Vol. 177, 2020, pp. 749
https://doi.org/10.1016/j.actaastro.2020.11.006

[21] Huang, J., Misra, A.K., "Controlled deployment of a long tether to operate as a partial space elevator", Astrodynamics, Vol. 8, No. 2, 2024, pp. 311–321.
https://doi.org/10.1007/s42064-024-0225-5

[22] Ledkov, A.S., Pikalov, R.S., "Nonlinear Control of Tether Retrieval in an Elliptical Orbit", *Russian Journal of Nonlinear Dynamics*, Vol. 19, No. 2, 2023, pp. 201-218
https://doi.org/10.20537/nd230401

[23] Wang, C., Wang, P., Li, A., Guo, Y., "Deployment of tethered satellites in low-eccentricity orbits using adaptive sliding mode control", *Journal Aerospace Engineering*, Vol. 30, No. 6, 2017, pp. 04017077.
https://doi.org/10.1061/(ASCE)AS.1943-5525.0000793

[24] Wang, W., Wu, Z., Liu, J., "Dynamic analysis of cislunar suspension tether swings", *Acta Astronautica*, Vol. 216, 2024, pp. 350-369.
https://doi.org/10.1016/j.actaastro.2024.01.010

[25] Yu, B.S., Zhu, Z.H., "Symmetric and asymmetric dynamics of a tethered satellite in nontypical planes", *Acta Astronautica*, Vol. 202, 2023, pp. 585-594.

https://doi.org/10.1016/j.actaastro.2022.11.019

[26] Luo, C., Wen, H., Jin, D., Sun, J., "Retargeting control of a multi-tethered satellite formation at sun-earth libration point", *Advances in Space Research*, Vol. 70, No. 2, 2022, pp. 268-285.
https://doi.org/10.1016/j.asr.2022.03.040

[27] Aslanov, V.S., "Tether System in Martian-Moons-eXploration-Like Mission for Phobos Surface Exploration", *Journal of Spacecraft and Rockets*, Vol. 61, No. 1, 2024, pp. 319-326.
https://doi.org/10.2514/1.A35777

[28] Szebehely, V., *Theory of orbits: the restricted three-body problem*, Academic Press, San Diego, CA, 1967.

[29] Kluever, C. A., *Space flight dynamics*, John Wiley & Sons, 2018.

[30] Scheeres, D. J., Olikara, Z., Baresi, N., "Dynamics in the Phobos environment", *Advances in Space Research*, Vol. 63, No. 1, 2019, pp. 476-495.
https://doi.org/10.1016/j.asr.2018.10.016

[31] Chen H., Hou X., Bando M., "Towards stable orbiting around small moons using the J2-perturbed elliptic-restricted three-body problem", *Journal of Guidance, Control and Dynamics*, Vol.47, No. 7, 2023, pp. 1327-1340
http://dx.doi.org/10.2514/1.G008001

[32] Rambaux, N., Castillo-Rogez, J. C., Le Maistre, S., Rosenblatt, P., "Rotational motion of Phobos", *Astronomy & Astrophysics*, No. 548, 2012, pp. A14.
http://dx.doi.org/10.1051/0004-6361/201219710

[33] Wählisch, M., Willner, K., Oberst, J., Matz, K.-D., Scholten, F., Roatsch, T., Hoffmann, H., Semm, S., Neukum, G., "A new topographic image atlas of Phobos", *Earth and Planetary Science Letters*, Vol. 294 No. 3-4, 2010, pp. 547-553.
https://doi.org/10.1016/j.epsl.2009.11.003

[34] Kuzmin, R.O., Shingareva, T. V., Zabalueva, E. V., "An engineering model for the Phobos surface", *Solar System Research*, Vol.37, 2003, pp. 266-281.
https://doi.org/10.1023/A:1025074114117

[35] Basilevsky, A. T., Lorenz, C. A., Shingareva, T. V., Head, J. W., Ramsley, K.R., Zubarev, A. E., "The surface geology and geomorphology of Phobos", *Planetary and Space Science*, Vol. 102, 2014, pp. 95-118.
https://doi.org/10.1016/j.pss.2014.04.013

[36] Karachevtseva, I. P., Oberst, J., Zubarev, D. V., Nadezhdina, I. E., Kokhanov, A. A., Garov, A. S., Uchaev, D.V., Malinnikov V. A., Klimkin, N.D., "The Phobos information system", *Planetary and Space Science*, Vol.102, 2014, pp. 74-85.

https://doi.org/10.1016/j.pss.2013.12.015

[37] Nakamura, T., Ikeda, H., Kouyama, T., Nakagawa, H., Kusano, H., Senshu, H., Kameda, S., Matsumoto, K., Gonzalez-Franquesa, F., Ozaki, N., Takeo, Y., “Science Operation Plan of Phobos and Deimos from the MMX Spacecraft”, *Earth Planets Space*, Vol. 73, No. 1, 2021, pp. 1–27.
https://doi.org/10.1186/s40623-021-01546-6